Macromolecular Journals

Macromolecular Materials and Engineering

Improvement of the Mechanical Properties and Creep Resistance of SBS Block Copolymers by Nanoclay Fillers

Siljana Lietz, Jing-Lei Yang, Eva Bosch, Jan K. W. Sandler, Zhong Zhang, Volker Altstädt*

SBS nanocomposites based on a SBS triblock copolymer containing different weight fractions of a commercial Cloisite 20A organoclay were prepared by melt-processing. Extensive electron microscopy as well as WAXS and static tensile and tensile creep tests were used to evaluate the resulting morphological and mechanical properties of the nanocomposites. The nanocomposite morphology is characterized by a combination of intercalated and partly exfoliated clay platelets with occasional clay aggregates present at higher clay contents; nanocomposite features that are reflected by the results of both the static tensile as well as the tensile creep tests at room temperature. For this particular thermoplastic elastomer nanocomposite system, well dispersed nanoclays lead to an enhanced stiffness and ductility; effects that induce promising improvements in nanocomposite creep performance.

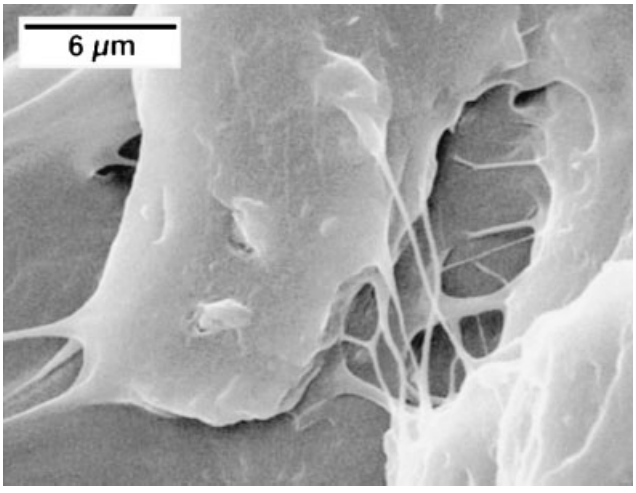

Introduction

Thermoplastic elastomers (TPEs) are characterized by remarkable mechanical (stiffness, strength, toughness, etc.) and haptic properties as well as by generally good processing characteristics similar to those of conventional thermoplastics. Among the TPEs, the polystyrene-*block*-polybutadiene-*block*-polystyrene triblock copolymer (SBS) has the greatest commercial relevance, reflected by about 50% of the worldwide consumption of all TPEs, due to its good performance level and low price compared to other common TPE grades.[1] Owing to the widely separated glass transition temperatures (T_g) of the constituent phases, SBS triblock copolymers provide a broad range of service temperatures.[2] Their significance concerning technical applications lies in the fact that, at room temperature, the flexible rubbery blocks ($T_g \approx -80\,^{\circ}C$) are anchored on both sides by glassy chain ends ($T_g \approx 100\,^{\circ}C$). Moreover, through variation of the molecular weight, composition, chain architecture and processing conditions, the phase separation behavior as well as the dimensions

S. Lietz, E. Bosch, J. K. W. Sandler, V. Altstädt
Polymer Engineering, University of Bayreuth, 95447 Bayreuth, Germany
Fax: +49 921 55 7473; E-mail: altstaedt@uni-bayreuth.de
J.-L. Yang, Z. Zhang
Institute for Composite Materials, University of Kaiserslautern, 67663 Kaiserslautern, Germany
Z. Zhang
National Center for Nanoscience and Technology of China, 100080 Beijing, China

DOI: 10.1002/mame.200600280

and orientations of the microdomains and, consequently, the resulting mechanical performance can be accurately controlled.[3]

Up to now, the creep resistance, permanent set, and compression set resistance of all TPE classes are usually still inferior to those of comparable cured rubbers (especially at elevated temperatures) so that SBS for example cannot be used for demanding applications such as tires.[1] One method of improving the creep resistance presented by Blackwell and Mauritz is the use of sulfonated polystyrene-*block*-poly(ethylene-*co*-butylene)-*block*-polystyrene (sSEBS) block copolymers.[4] However, the commercial exploitation of sSEBS requires the design and construction of tailored production lines, a cost-intensive approach.

Another promising method to improve the mechanical properties of TPEs in general is the addition of nanoparticles, especially of layered silicate clays. In recent decades, fundamental research has shown that such polymer-clay nanocomposites frequently exhibit unexpected properties synergistically derived from the two phases.[5–8] Depending on the degree of intercalation of the polymer chains into the gallery spacing of the clays, nanocomposites are obtained with structures ranging from an intercalated to a fully exfoliated state. It has been demonstrated that various factors such as the method of preparation, the structure and polarity of the virgin polymer, the source of the clay, as well as the length and number of alkyl groups of the cationic modifier molecule, etc. strongly influence the final morphology of such nanocomposites.[9–12] Due to the ability of the polystyrene (PS) to intercalate well into suitably modified layered silicates and the resulting enhancement of the thermal and thermomechanical properties, several research groups have investigated the morphology as well as the solid-state thermal and mechanical properties of SBS nanocomposites.[13–19] However, the microstructure evolution and resulting performance of these thermoplastic elastomer nanocomposites also critically depend both on the composition of the matrix as well as on the modification of the silicate clays.[16,18–20]

Numerous studies have focused on the mechanical properties and deformation mechanisms of nanocomposites using thermoplastics as well as thermoplastic elastomers as matrices.[7,9,10,16–21] However, comparatively little attention has been paid to the creep behavior of such nanocomposites although several groups have demonstrated that the improvement of mechanical properties of polymers such as stiffness by the addition of various nanoparticles is related to an enhanced creep performance.[7,9,22–25] In addition, the presence of finely-dispersed nanoparticles is expected to enhance the creep performance of polymers on a fundamental level, as the filler particles strongly influence the polymer chain mobility.[24]

Previously, we demonstrated the effect of different commercial organoclay structures on the morphology as well as the resulting mechanical and deformation behavior of SBS nanocomposites using a star-shaped SBS block copolymer with a comparatively high PS content.[20] As an extension of this approach, it is the objective of this study to evaluate the correlation between the static tensile and tensile creep resistance and the morphology of such SBS-clay nanocomposites obtained by melt-processing. There is as yet no systematic study regarding the mechanical behavior of SBS-clay nanocomposites under such loading conditions, although an enhancement of these properties could significantly broaden the application spectrum of this particular thermoplastic elastomer.

Experimental Part

Materials and Sample Preparation

The chosen SBS block copolymer, provided by BASF AG, is a star block copolymer with an average molecular weight $\overline{M}_w$ of 91 800 $g \cdot mol^{-1}$ and a polydispersity index of about 2. The stars generally have four arms; each arm consists of polybutadiene blocks as a core and PS blocks as outer arms. The block copolymer has a total styrene volume fraction of 0.74. Details regarding the polymer matrix are summarized in Table 1.

The layered silicate clay used in this study is a commercial organoclay (Cloisite 20A), supplied by Southern Clay Products, USA. The natural montmorillonite (MMT) is organically modified with dimethyl dihydrogenated-tallow ammonium with a cation-exchange capacity (CEC) of 95 mequiv. per 100 g clay as compared to the CEC of 92 mequiv. per 100 g clay of the sodium ion in the native clay.[26] Replacing the sodium ions with the larger ammonium cations leads to an increase of the interlayer spacing (d_{001}) to a value of about 2.4 nm.[26]

The block copolymer and different weight fractions of the organoclay (1.5 and 3 wt.-% MMT, respectively) were melt-compounded using a co-rotating, intermeshing twin-screw extruder (Berstorff ZE 25). It should be noted that the clay contents correspond to the weight fraction of inorganic silicate filler, as the silicate is the reinforcing component. Prior to the extrusion step, the organoclay powder and the SBS pellets were

Table 1. Characteristics of the SBS block copolymer under investigation.

SBS type	$\overline{M}_w$ / $g \cdot mol^{-1}$	$\overline{M}_w/\overline{M}_n$	Molecular structure
SBS	91 800	1.99	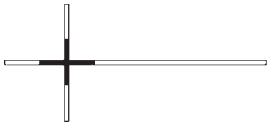

Macromolecular Journals
DOI: 10.1002/mame.200600280

thoroughly mixed in a container. Compounding was carried out at an extruder barrel temperature of 190 °C, a die temperature of 210 °C, and at a screw speed of 120 rpm corresponding to a mean residence time of 1 min. Extruded and quenched nanocomposite pellets were dried and then injection-molded into standard tensile bars of 2 mm thickness (specimen type 5A DIN EN ISO 527-2) using an Arburg Allrounder 420 C 800-250 injection-molding machine operating at 210 °C, with a mould temperature of 70 °C, an injection pressure of 700 bar, and a holding pressure of 700 bar.

Characterization

Wide-Angle X-Ray Scattering (WAXS)

WAXS experiments were carried out in order to evaluate the clay interlayer distance in the injection-molded SBS nanocomposites as a function of the clay content. 1-dimensional (1D) WAXS patterns were recorded using a Seifert ID 3000 diffractometer operating at a generator voltage of 40 kV and a generator current of 50 mA in the reflection mode, using an incident X-ray wavelength of 1.542 Å and a scan rate of $0.3^\circ \cdot \text{min}^{-1}$.

Transmission Electron Microscopy (TEM)

The dispersion of the clays in the various nanocomposites was further examined using a transmission electron microscope from Zeiss CEM 902 A EFTEM, operating at 80 kV. Samples for the TEM analysis were prepared from the central cross-section of the extruded pellets normal to the flow direction. Ultra-thin sections of approximately 50 nm in thickness were cryo-cut using a Reichert-Jung Ultracut E microtome and a diamond knife at −50 °C. Subsequently, the polybutadiene phase was selectively stained using osmium tetroxide (OsO_4) for 1 min following a procedure described in ref.[27]

Tensile Tests

Tensile tests were conducted according to DIN EN 527-2 using a Zwick Z020 tensile machine operating at room temperature. In order to accurately determine the tensile modulus and yield stress, a crosshead speed of 1 $\text{mm} \cdot \text{min}^{-1}$ and a macro-extensometer were used. The stress and elongation at break, respectively, were obtained at a crosshead speed of 5 $\text{mm} \cdot \text{min}^{-1}$. At least eight specimens of each composition were tested.

Tensile Creep Tests

Uniaxial tensile creep tests were performed using a Creep Rupture Test Machine equipped with a double lever system (Coesfeld GmbH, Model 2002). Ten specimens can be measured simultaneously in an environmental chamber. Prior to testing, the desired constant load for each measurement channel was calibrated using a force transducer. The samples were fixed into the clamps without loading. A gauge length of 10 mm was marked on each specimen and the elongation was monitored as a function of the time using a video camera equipped with a step-controlled motor connected to a computer image analysis system during the whole period of the creep test. Two constant stresses, i.e., 8.5 and 20 MPa, were applied at 23 °C. Two specimens were tested for each stress level and the mean values are presented. The creep compliance of the different specimens was calculated by taking the ratio of the measured creep strain and the initial stress. The measurement procedure was performed in accordance with ASTM 2990-01.

Scanning Electron Microscopy (SEM)

Following tensile testing, specimen fracture surfaces were analyzed by SEM using a JEOL JSM-IC 848 operating at 10 kV. In order to avoid electrostatic charging, the fracture surfaces were gold coated (15 nm in thickness) by ion sputtering.

Results and Discussion

A comparative evaluation of melt-processed SBS-clay nanocomposites based on this particular star-shaped SBS block copolymer has previously demonstrated that the morphology of such nanocomposites critically depends on the surface modification of the clays.[20] Whereas a more hydrophilic commercial Cloisite 30B could not be dispersed in this matrix under these processing conditions, the more hydrophobic Cloisite 20A led to partly exfoliated, partly intercalated nanoclays. This particular nanocomposite microstructure was independent of further processing steps following the twin-screw compounding; subsequently, the injection-molded tensile bars containing the Cloisite 20A remained transparent with just a slight darkening of the yellowish color.

Nanocomposite Morphology

Representative 1-dimensional wide-angle X-ray diffraction (XRD) patterns of the neat SBS and the SBS nanocomposites containing 1.5 and 3 wt.-% of the organoclay, respectively, are shown in Figure 1. All scattering intensities are normalized to the intensity of the amorphous polymer halo. As can be seen, the nanocomposite patterns reveal a broad shallow peak of low intensity at 2θ values of around 2.1 and 2.2° for the 1.5 and 3 wt.-% content of organoclay, respectively. These WAXS reflections correspond to interlayer spacing of $d_{001} = 4.20$ and 4.02 nm of the incorporated organoclay, respectively. Comparing these gallery spacing to the initial value of 2.4 nm of the organoclay in the as-received state[26] and taking into account the width of the reflection which normally broadens with an increasing disorder of the intercalation,[9] it appears that both nanocomposites consist of an intercalated clay structure with a high degree of disorder of the individual platelets.

However, the detailed TEM provided evidence for a mixed microstructure in the SBS nanocomposites, inde-

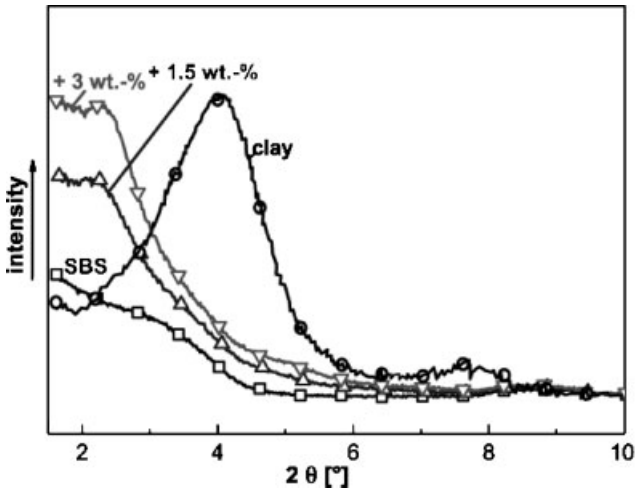

Figure 1. Representative WAXS patterns for SBS nanocomposites with increasing organoclay (Cloisite 20A) content. Data for the as-received clay is shown for comparison.

pendent of the clay content (Figure 2). In addition, these TEM micrographs also verify the generally good distribution and dispersion of the organoclay in the SBS matrix under the chosen processing conditions. Although the micrographs at higher magnification (Figure 2c and 2d) clearly reveal remaining clay stacks consisting of three to five clay layers for both SBS nanocomposites containing 1.5 and 3 wt.-% of organoclay, a significant degree of exfoliation can be observed.

These observations with regard to the delamination and dispersion of suitably modified organoclays in a SBS matrix are in good agreement with those reported by Liao et al. and Xu et al.[18,19] Using a linear as well as a star-shaped SBS with a PS phase fraction of 30%, both intercalated and partly exfoliated SBS nanocomposites were obtained.[18,19] A low intercalation efficiency as well as a less pronounced dispersion of silicate stacks was reported for non-matched SBS-clay systems.[18,19] Although both the particular functionalization of the commercial clay as well as the polymer matrix itself play an important role in achieving the clay dispersion reported here, no fully exfoliated nanocomposite morphology as described for an amino-functionalized PS modification in SBS was achieved.[16]

Mechanical Properties

Representative engineering tensile stress versus strain curves of the neat SBS and the SBS nanocomposites measured at room temperature are presented in Figure 3. The corresponding characteristic values of these tests are further summarized in Table 2. As for poly(propylene)-clay nanocomposites,[21] the yield stress of the SBS is only slightly influenced by the addition of the organoclay while there is some improvement in tensile modulus (Figure 3a). Furthermore, comparable effects for SBS nanocomposites were reported by Ha et al.[16]

The mechanical behavior of such nanocomposites in the elastic and viscoelastic deformation range is dominated by the PS lamellae if the SBS block copolymer contains alternating PS and PB lamellae or if the PB microdomains are embedded in the PS.[16] In the presence of the clay platelets, the lamellar alignment of the PS microdomains is reduced.[16] In addition, the clay platelets (or stacks) themselves are not always preferentially oriented to the loading direction. Although there is some straightforward mechanical reinforcement due to the clays, the intrinsic properties of the matrix are somewhat degraded and, as a result, the increases in tensile modulus and yield stress are moderate. In agreement with the simulation results presented in ref.[16], it is assumed that both the clay stacks as well as the individual clay platelets induce an imperfect arrangement and lower degree of alignment of the PB hexagonal cylinders dispersed in the PS phase.

Yet, a pronounced increase in ultimate strength and elongation at failure for both nanocomposites as compared to the neat matrix was observed Figure 3b. The ultimate elongation at room temperature is trebled with the addition of 3 wt.-% of the organoclay, although there is little additional benefit over the 1.5 wt.-% loading fraction, again in agreement with the literature.[19] Nevertheless, these thermoplastic elastomer nanocomposites reveal clear improvements in ultimate strength and ductility whereas the addition of such organoclays to more standard thermoplastics such as poly(propylene) and polyamide-6 often leads to a severe degradation of the ductility and toughness.[28,29]

Further evidence for the significantly altered micromechanical deformation behavior of the SBS nanocomposites explaining the observed improvements in composite ductility is provided by the representative scanning electron micrographs of fracture surfaces shown in Figure 4. In comparison to the rather featureless fracture surface of the neat SBS (Figure 4a), significant fibrillation of the SBS matrix takes place with the addition of 1.5 wt.-% organoclay (Figure 4b). This fibrillation is a result of the good interfacial bonding between the organoclay and the matrix and also reflects the good dispersion of the filler. Similar improvements in the ability of the polymer matrix to plastically deform by multiple microvoiding and subsequent fibrillation as a result of the addition of nanoclays have also been reported for particular poly(propylene) and polyamide clay nanocomposites.[21,30] These variations in the overall mechanical performance of polymer nanocomposites clearly indicate that both the nature of the matrix itself as well as the resulting degree of clay dis-

Macromolecular Journals
DOI: 10.1002/mame.200600280

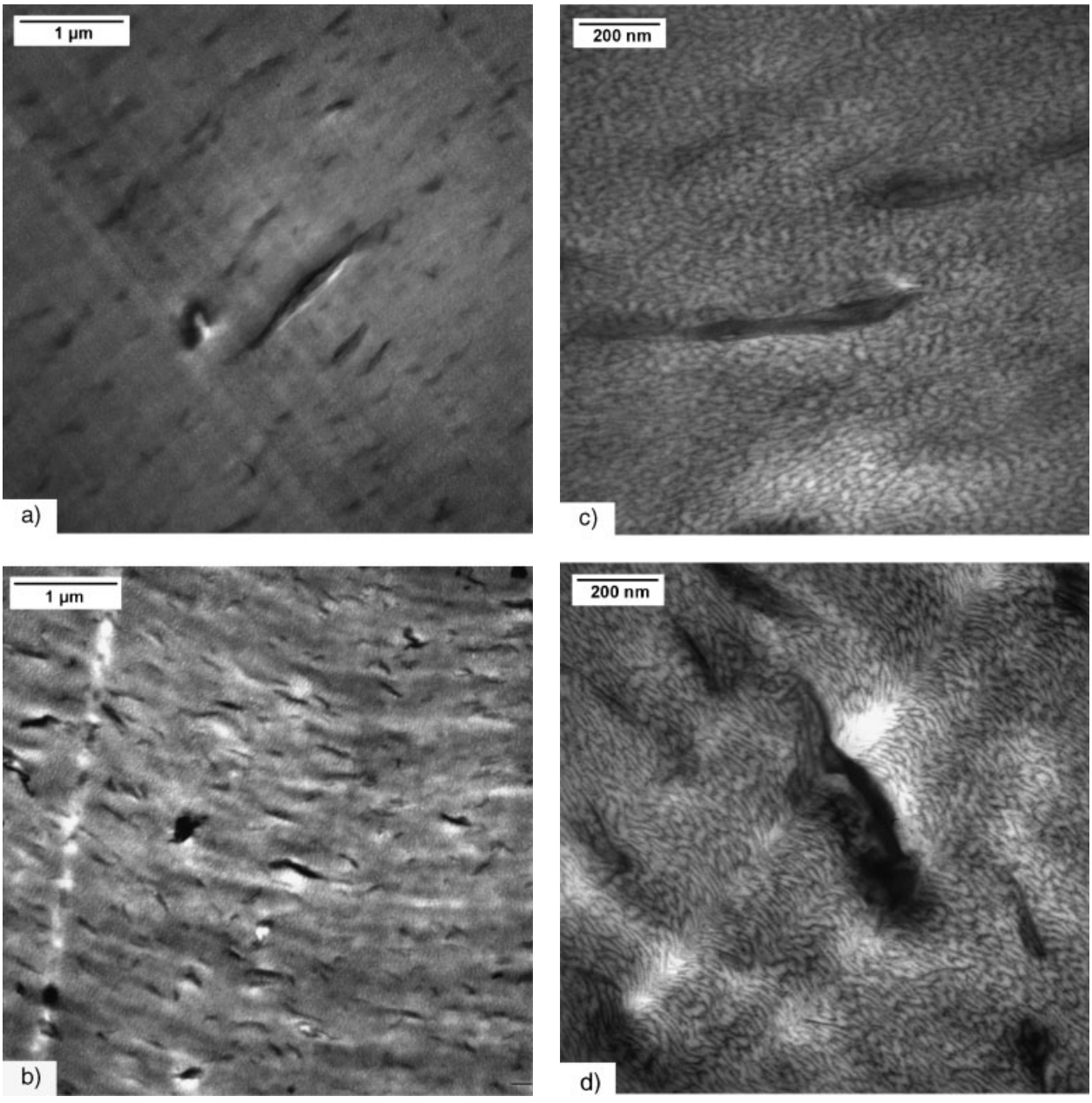

Figure 2. Representative TEM micrographs of SBS nanocomposites containing a) 1.5 and b) 3 wt.-% of organoclay (Cloisite 20A). The micrographs in c) and d) further highlight the partly intercalated, partly exfoliated clay morphology for the SBS nanocomposites containing 1.5 and 3 wt.-%, respectively.

persion and the interparticle distance as a function of the clay content are important factors.[21,31,32]

In line with this argument, both the static tensile test results as well as the fracture surface analysis indicate that the deformation behavior of the SBS nanocomposites depends on the degree of clay intercalation and exfoliation as well as on the general quality of the distribution and dispersion.[20] The SEM micrographs of the 3 wt.-% nanocomposite (Figure 4c) with the higher volume fraction of intercalated clay stacks (and a correspondingly reduced interparticle distance) indicate that plastic stretching still occurs; however, the formation of voids limits the overall drawability. Although it could not be resolved by the previously discussed analysis of the nanocomposite microstructure using TEM and WAXS, the SEM micrographs of the 3 wt.-% nanocomposite clearly show the presence of some remaining clay aggregates (Figure 4c). These aggregates in turn explain the observed tensile behavior of these

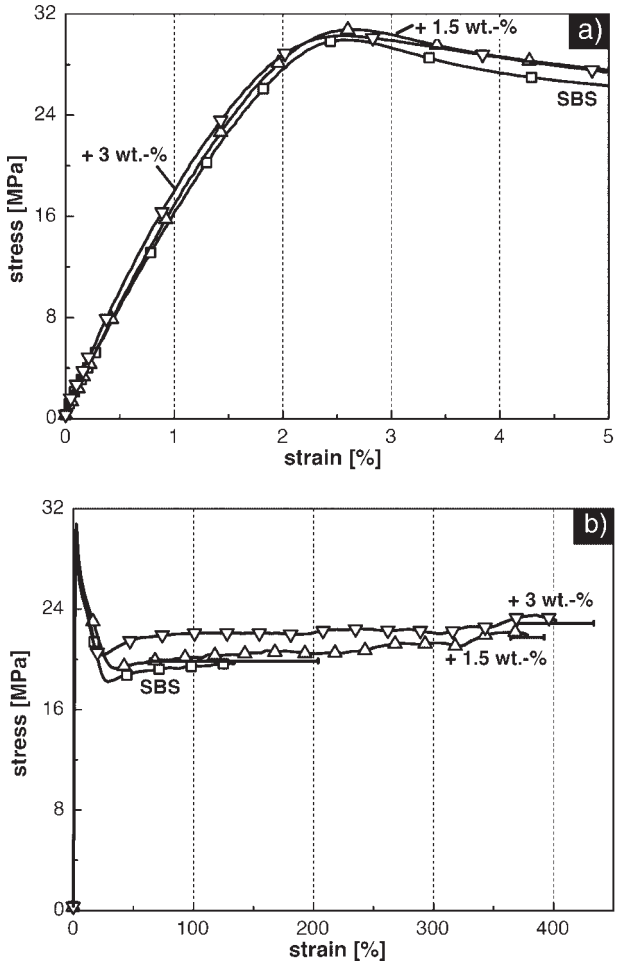

Figure 3. Representative engineering stress-strain diagrams of SBS nanocomposites as a function of the organoclay (Cloisite 20A) content at room temperature covering a) the low strain regime (<5%) and b) the whole strain regime.

nanocomposites as compared to both the neat matrix and the 1.5 wt.-% system. In a soft matrix, such aggregates provide a stiffening effect; however, the strength enhancement is limited as compared to the partly intercalated, partly exfoliated morphology observed for the nanocomposite with the lower nanoclay content. Although such aggregates act as stress concentration sites initiating multiple microvoiding they nevertheless do not detrimentally affect the overall ductility of the nanocomposite system.

Creep Response and Modeling Analysis

In addition to the static tensile tests, creep measurements were carried out in order to evaluate the creep resistance and dimensional stability of the SBS-clay nanocomposites compared to the neat SBS. The creep performance of the neat SBS and the SBS-clay nanocomposites is characterized by the creep strain ε as well as by the creep compliance J as a function of creep time t, respectively, under a constant stress. In order to describe this time-dependent behavior, many mathematical models have been evaluated, as summarized in ref.[33] The Findley power law and the 4-element model (Burgers model) especially are often used to describe the creep behavior of polymers and polymer composites as they generally show good agreement with experimental data.[34] A detailed description of the tensile creep behavior of polymers in general is provided by Yang et al.;[24,25] however, the two models used in this study are briefly introduced here.

The Burgers model consists of two springs and two dashpots, as shown schematically in Figure 5. According to this model, the total strain ε_B at a time t is given as follows:

$$\varepsilon_B = \frac{\sigma_0}{E_1} + \frac{\sigma_0}{E_2} * \left(1 - e^{\frac{-t}{\tau}}\right) + \frac{\sigma_0}{\eta_1} t, \quad (1)$$

where E_1 and η_1 are the modulus and the viscosity of the Maxwell spring and dashpot, respectively; E_2 and η_2 are the modulus and the viscosity of the Kelvin spring and dashpot, respectively. σ_0 is the initially applied stress while $\tau = \eta_2/E_2$ is defined as the retardation time. As indicated by Equation (1), the total strain ε_B is a combination of three contributions. Hooke's strain $\varepsilon_H = \sigma_0/E_1$ characterizes the linear deformation which occurs immediately at the start of the creep experiment. The Newtonian strain $\varepsilon_N = \sigma_0/\eta_1$ reflects the viscous behavior whereas the Voigt-Kelvin

Table 2. Summary overview of relevant tensile properties of the neat SBS and the SBS-clay nanocomposites at room temperature.

Sample	Young's modulus	Yield stress	Tensile strength	Tensile stress at break	Elongation at break
	MPa	MPa	MPa	MPa	%
SBS	1 744 ± 119	30.4 ± 0.7	30.4 ± 0.7	19.1 ± 0.7	134 ± 70
SBS + 1.5 wt.-%Cloisite 20A	1 795 ± 12	30.1 ± 0.6	30.1 ± 0.6	21.8 ± 0.3	373 ± 14
SBS + 3 wt.-%Cloisite 20A	1 932 ± 79	30.9 ± 0.5	30.9 ± 0.5	23.1 ± 0.2	395 ± 31

DOI: 10.1002/mame.200600280

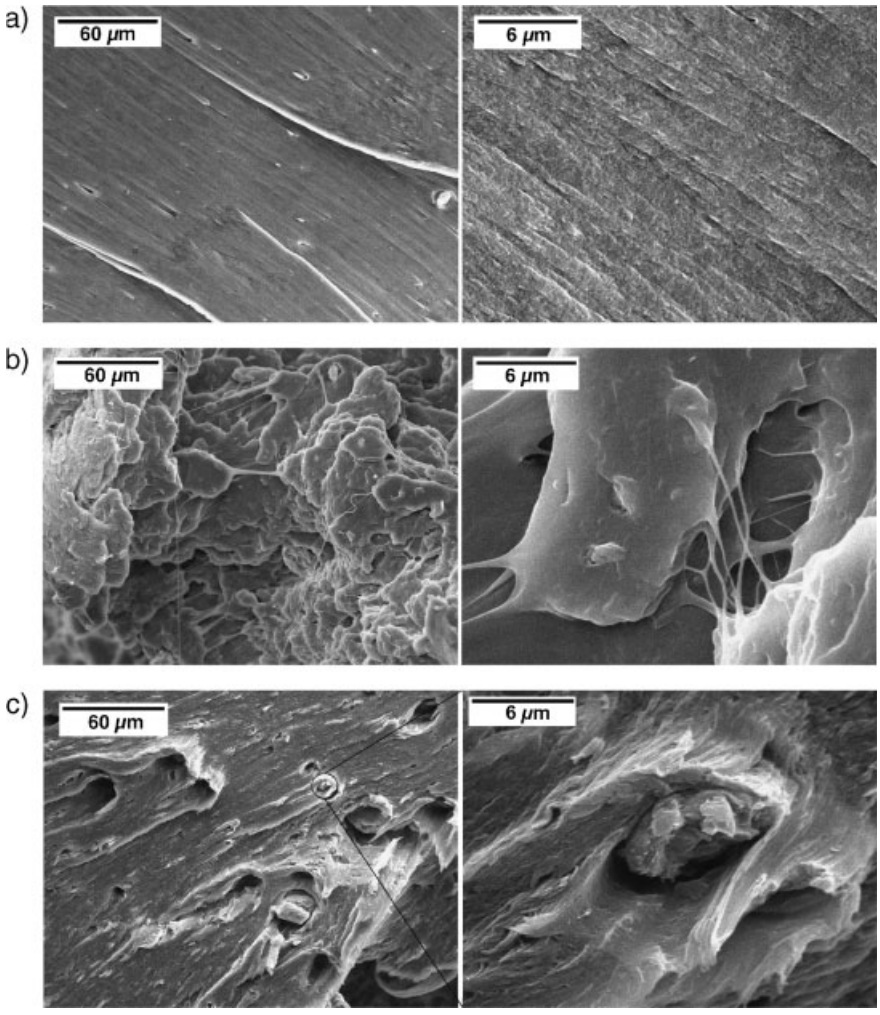

Figure 4. Representative SEM micrographs of fracture surfaces following tensile testing of the a) neat SBS and the SBS nanocomposites containing b) 1.5 wt.-% and c) 3 wt.-% of organoclay (Cloisite 20A), respectively.

strain $\varepsilon_{V\text{-}K}$, corresponding to the second term in Equation (1), is related to the viscoelastic behavior of the material. A systematic variation of the simulation parameters to fit the experimental data will consecutively show the effect of the nanofillers on the various strain contributions.

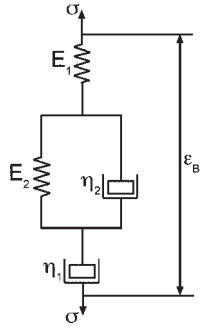

Figure 5. Schematic diagram of Burgers model.

Compared to the Burgers model, the total creep strain ε_F as a function of the time t in the Findley power law has a much simpler expression, given by

$$\varepsilon_F = \varepsilon_0 + \varepsilon_1 t^n, \quad (2)$$

where n is a constant independent of the stress and generally is less than one. ε_0 is the time-independent strain, and ε_1 is the coefficient of the time-dependent term. ε_0 and ε_1 are a function of the stress and other environmental variables including temperature, moisture, etc.

The creep performance of the neat SBS and the SBS-clay nanocomposites was investigated at room temperature under two stress levels corresponding to 28% and 67% of the ultimate tensile stress (UTS) of the neat SBS matrix, respectively. The experimental results of the creep strain versus creep time measurements at an applied stress of 8.5 MPa are presented in Figure 6. The initial rapid elongation seen for all specimens is due to a mainly elastic and partly viscoelastic/plastic deformation of the materials as soon as the creep stress is applied and is independent of time.[24] Following an incubation period, the creep rate reaches a steady state. This secondary creep

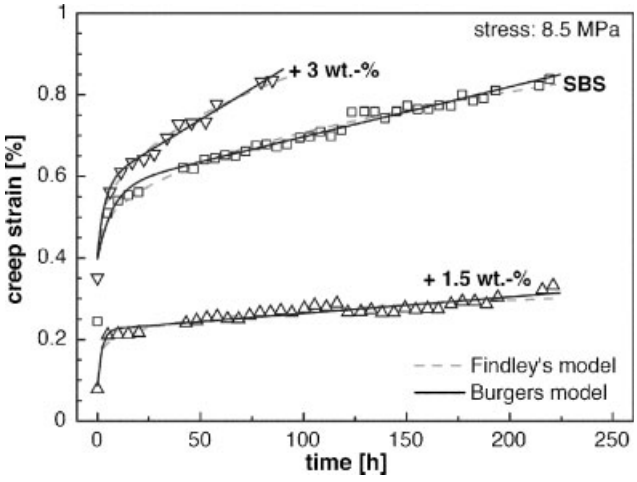

Figure 6. Tensile creep strain versus test duration curves of the SBS nanocomposites at 8.5 MPa (28% of the static UTS of the neat SBS) at room temperature.

stage was observed for up to 200 h. In these experiments, the specimens did not fail.

As can be seen, within the observation period, the nanocomposite containing 1.5 wt.-% of the organoclay reveals a significantly reduced creep strain and creep rate as compared to the neat SBS. These observations clearly indicate an enhanced creep resistance as a result of the addition of the well-dispersed organoclay. However, increasing the clay content to 3 wt.-% changes the creep behavior again. It is noteworthy to point out that the creep resistance of this nanocomposite is even reduced as compared to the neat SBS in terms of an increased deformation and creep rate, reflecting the generally lower quality of dispersion and distribution of the intercalated clay stacks and the presence of aggregates acting as stress concentrators.

The Burgers model and Findley power law were comparatively used to analyze the creep performance of the systems in more detail.[34] As shown in Figure 6, both modeling approaches lead to a satisfactory agreement with the experimental data. The used simulation parameters are summarized in Table 3 and further highlight the beneficial effect of the low nanoclay content on the creep resistance of SBS under these test conditions.

In the Burgers model, the elastic behavior is given by the parameter E_1. The nanocomposite containing 1.5 wt.-% of dispersed organoclays shows a much higher value for E_1, indicating a higher stiffness as compared to the neat matrix. A further increasing clay content leads to a decreased elasticity of the system and induces a higher initial elongation at the start of the creep experiment as compared to the neat SBS. In addition, the viscoelastic behavior – as given by η_2 and by E_2 – of the SBS is also affected by the presence of the organoclays. Again, the 1.5 wt.-% nanocomposite shows the highest E_2 value, indicating the smallest deformation during the transition from the primary to the secondary creep stage. The short retardation time as given by the ratio of η_2 to E_2 for the nanocomposite containing 1.5 wt.-% of organoclay further verifies that the transition period from the primary to the secondary creep stage is consistent with the improved dimensional stability seen for this particular nanocomposite. Indeed, a further increase of the clay content has a detrimental effect on the creep performance. The SBS nanocomposites containing 3 wt.-% of organoclay exhibits the highest ratio of η_2 to E_2, reflecting the most prominent viscoelastic behavior. In addition, the viscosity of the Maxwell dashpot η_1 is higher by several orders of magnitude than that of the Kelvin dashpot for all materials. This fact implies that the viscosity of the bulk material is mainly controlled by η_1, rather than by η_2. The finely dispersed clays in case of the 1.5 wt.-% nanocomposite lead to a significantly higher viscosity η_1 and, therefore, to a smaller deformation in a definite time period as compared to both the neat matrix and the 3 wt.-% nanocomposite, as the aggregates reduce the viscosity of the whole system.

As indicated by the data for the Findley power law, the addition of 1.5 wt.-% of nanoclay significantly reduces the values of ε_0, ε_1, and n in comparison to both the neat SBS as well as to the nanocomposite with the higher clay loading, mirroring the trends discussed so far.

The creep compliance of the SBS-clay nanocomposites as a function of the time is illustrated in Figure 7. Again, the SBS nanocomposite containing 1.5 wt.-% of the organoclay shows a distinct reduction of the creep compliance as compared to the neat SBS. Besides an increased creep compliance, the development of the creep compliance as a function of the creep time shows a different behavior when adding 3 wt.-% of the organoclay. The slope of the creep compliance is reduced at the beginning of the creep test and increases with increasing creep duration at this stress level.

The creep test results of all systems at an applied stress level of 20 MPa are summarized in Figure 8. Due to the high stress level, all specimens show a tertiary creep stage directly and failed in a relatively short time with extensive necking. However, the creep resistance of the 1.5 wt.-% nanocomposite again is significantly better than that of the neat SBS and the nanocomposite with the higher clay content. Yet, at this high stress level, the 3 wt.-% nanocomposite also shows a positive effect of the clay reinforcement compared to neat matrix as the creep lifetime of the nanocomposites is greatly prolonged.

Table 3. Calculated parameters from Burgers model and Findley power law at a creep stress of 8.5 MPa at room temperature.

Sample	Burgers model					Findley power law		
	E_1	E_2	η_1	η_2	τ	ε_0	ε_1	n
	MPa	MPa	GPa · h	GPa · h	h	%	10^{-4} $h^{1/n}$	
SBS	2 349	4 749	682	19.1	4.03	0.398	4.94	0.401
SBS + 1.5 wt.-% Cloisite 20A	8 026	7 582	1653	9.67	1.28	0.134	3.42	0.314
SBS + 3 wt.-% Cloisite 20A	1 930	5 807	289	29.7	5.11	0.424	6.11	0.430

Macromolecular Journals
DOI: 10.1002/mame.200600280

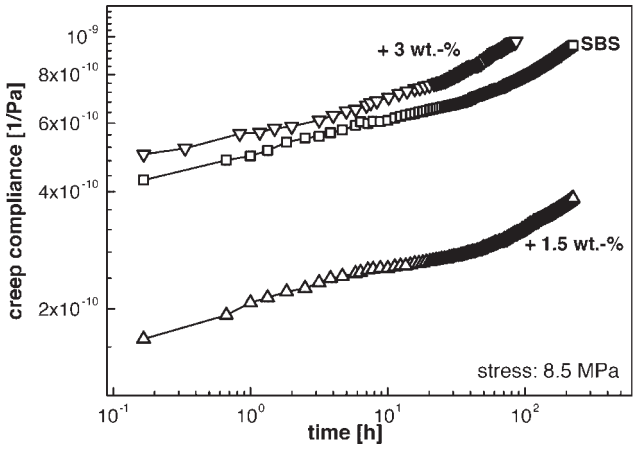

Figure 7. Creep compliance versus test duration curves of the SBS nanocomposites at 8.5 MPa (28% of the static UTS of the neat SBS) at room temperature.

As stated in ref.[24,25], two key factors related to an improved creep performance of polymer nanocomposites are an enhanced stiffness of the nanocomposites as well as a good interfacial bonding of the organoclay and the matrix. Taking into account the higher modulus of the SBS nanocomposite containing 3 wt.-% of Cloisite 20A, the different creep behavior as a function of the organoclay weight fraction appears to be related to the different deformation behavior of the SBS nanocomposites as discussed in the context of the tensile tests.

The larger number of bigger clay stacks as well as the occasional presence of small aggregates in the SBS nanocomposites containing 3 wt.-% Cloisite 20A leads to void formation which consequently enhances the creep rate. Although some interfacial bonding of the polymer matrix to the remaining clay aggregates can be assumed,

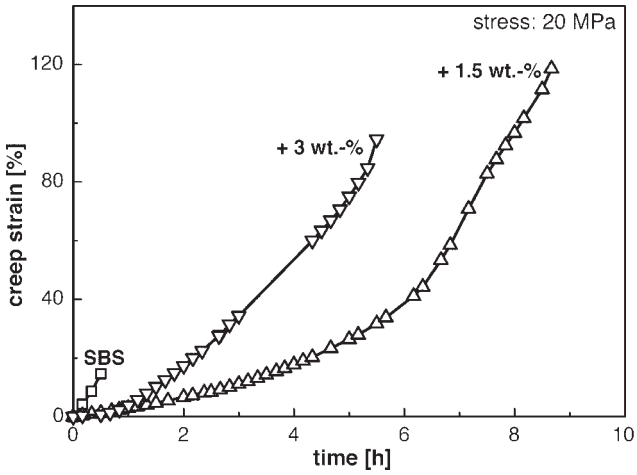

Figure 8. Tensile creep strain versus test duration curves of the SBS nanocomposites at 20 MPa (67% of the static UTS of the neat SBS) at room temperature.

the shear stresses during deformation are expected to induce slippage in the aggregates whereby the creep resistance is impaired at lower stress levels and small corresponding deformations.[24] Yet, in the case of a high stress level, these aggregates nevertheless restrict the mobility of polymer chains and thereby improve the creep resistance. In contrast, the homogeneous distribution of 1.5 wt.-% Cloisite 20A as single clay platelets or stacks of two or three intercalated clay platelets leads to pronounced fibril formation due to the altered micromechanical deformation behavior and, therefore, to the observed reduction of creep rate and strain, independent of the stress level.

Conclusion

Polystyrene-*block*-polybutadiene-*block*-polystyrene triblock copolymer (SBS) nanocomposites containing different contents of a commercial organoclay were prepared by twin-screw extrusion. Detailed morphological studies by electron microscopy as well as WAXS studies indicated a homogeneous dispersion and distribution of partly intercalated and partly exfoliated clay platelets for SBS nanocomposite containing 1.5 wt.-% Cloisite 20A. Comparable SBS nanocomposite containing 3 wt.-% of the Cloisite 20A showed a similar morphology, although occasional small aggregates could also be observed in this case.

Static tensile tests at room temperature revealed an enhanced tensile modulus as well as a significantly increased ductility of the thermoplastic elastomer with an increasing clay weight fraction. The nanocomposite tensile strength, however, strongly reflected the variations in clay dispersion with the particle aggregates at the 3 wt.-% loading fraction limiting the further enhancement of properties. Similarly, the results of the static creep tests at different constant stress levels also reflected these variations in nanocomposite microstructure and deformation behavior. The enhanced stiffness and ductility of the SBS nanocomposite with the lower clay content (1.5 wt.-% MMT) led to a significantly enhanced creep performance and, therefore, a higher dimensional stability, independent of the applied stress level. In contrast, the higher clay content only improved the creep performance of the SBS matrix at high stress levels. In summary, such thermoplastic elastomer nanocomposites based on well-dispersed silicate nanoclays clearly show a promising potential towards enhancing the creep performance of such soft matrices for demanding applications.

Acknowledgements: Z. Z. is grateful to the *Alexander von Humboldt Foundation* for his Sofia Kovalevskaja Award, financed

by the *German Federal Ministry of Education and Research (BMBF)* within the German Government's "ZIP" program for investment in the future. All authors gratefully acknowledge financial support by the *Deutsche Forschungsgemeinschaft (DFG)*.

Received: July 13, 2006; Revised: September 26, 2006; Accepted: October 5, 2006; DOI: 10.1002/mame.200600280

Keywords: block copolymers; creep; morphology; nanocomposites; tension

[1] G. Holden, H. R. Kricheldorf, R. R. Quirk, "*Thermoplastics elastomers*", 3rd Ed., Hanser, Munich 2004, p. 517.
[2] G. Holden, "*Understanding thermoplastic elastomers*", Hanser, Munich 2000, p. 15.
[3] R. Adhikari, G. H. Michler, *Prog. Polym. Sci.* **2004**, *29,* 949.
[4] R. I. Blackwell, K. A. Mauritz, *Polym. Adv. Technol.* **2005**, *16,* 212.
[5] S. S. Ray, K. Yamada, M. Okamoto, A. Ogami, K. Ueda, *Chem. Mater.* **2003**, *15,* 1456.
[6] X. Kornman, R. Thomann, R. Mülhaupt, J. Finter, L. A. Berglund, *Polym. Eng. Sci.* **1992**, *42,* 1815.
[7] J. S. Shelley, P. T. Mather, K. L. DeVries, *Polymer* **2001**, *42,* 5849.
[8] T. Kashiwagia, R. H. Harris Jr, X. Zhang, R. M. Briber, B. H. Cipriano, S. R. Raghavan, W. H. Awad, J. R. Shields, *Polymer* **2004**, *45,* 881.
[9] H. R. Dennis, D. L. Hunter, D. Chang, S. Kim, J. L. White, J. W. Cho, D. R. Paul, *Polymer* **2001**, *42,* 9513.
[10] T. D. Fornes, D. L. Hunter, D. R. Paul, *Polymer* **2004**, *45,* 2321.
[11] A. C. Balazs, *Curr. Opin. Solid State Mater. Sci.* **2003**, *7,* 27.
[12] W. Gianelli, G. Ferrara, G. Camino, G. Pellegati, J. Rosenthal, R. C. Trombini, *Polymer* **2005**, *46,* 7037.
[13] S. Bourbigot, J. W. Gilman, C. A. Wilkie, *Polym. Degrad. Stab.* **2004**, *84,* 483.
[14] G. Chen, S. Liu, S. Chen, Z. Qi, *Macromol. Chem. Phys.* **2001**, *202,* 1189.
[15] B. N. Jang, C. A. Wilkie, *Polymer* **2005**, *46,* 2933.
[16] Y.-H. Ha, Y. Kwon, T. Breiner, E. P. Chan, T. Tzianetopoulou, R. E. Cohen, M. C. Boyce, E. L. Thomas, *Macromolecules* **2005**, *38,* 5170.
[17] M. Laus, O. Francescangeli, F. Sandrolini, *J. Mater. Res.* **1997**, *12,* 3134.
[18] M. Liao, J. Zhu, H. Xu, Y. Li, W. Shan, *J. Appl. Polym. Sci.* **2004**, *92,* 3430.
[19] H. Xu, Y. Li, D. Yu, *J. Appl. Polym. Sci.* **2005**, *98,* 146.
[20] S. Lietz, J. K. W. Sandler, E. Bosch, V. Altstädt, *Kautsch. Gummi Kunstst.* **2006**, *7–8,* 388.
[21] J. M. Gloaguen, J. M. Lefebvre, *Polymer* **2001**, *42,* 5841.
[22] Z. Zhang, J.-L. Yang, K. Friedrich, *Polymer* **2004**, *45,* 3481.
[23] D. P. N. Vlasveld, H. E. N. Bersee, S. J. Picken, *Polymer* **2005**, *46,* 12539.
[24] J.-L. Yang, Z. Zhang, A. K. Schlarb, K. Friedrich, *Polymer* **2006**, *47,* 2791.
[25] J.-L. Yang, Z. Zhang, A. K. Schlarb, K. Friedrich, *Polymer* **2006**, *47,* 6745.
[26] http://www.nanoclay.com/
[27] T. Kirschnick, A. Gottschalk, H. Ott, V. Abetz, J. Puskas, V. Altstädt, *Polymer* **2004**, *45,* 5653.
[28] A. Leuteritz, D. Pospiech, B. Kretzschmar, M. Willeke, D. Jehnichen, U. Jentzsch, K. Grundke, A. Janke, *Macromol. Symp.* **2005**, *221,* 53.
[29] T. D. Fornes, P. J. Yoon, D. L. Hunter, H. Keskkula, D. R. Paul, *Polymer* **2002**, *43,* 5915.
[30] G.-M. Kim, D.-H. Lee, B. Hoffmann, J. Kressler, G. Stöppelmann, *Polymer* **2001**, *42,* 1095.
[31] P. K. Mallick, Y. Zhou, *J. Mater. Sci.* **2003**, *38,* 3183.
[32] A. S. Zerda, A. J. Lesser, *J. Polym. Sci., Part B: Polym. Phys.* **2001**, *39,* 1137.
[33] E. Reichelt, *Kunststoffe* **1986**, *76,* 971.
[34] W. Grellmann, S. Seidler, "*Kunststoffprüfung*", Hanser, Munich 2005, p. 182.

DOI: 10.1002/mame.200600280